Minimization of Space Harmonics for Fractional-Slot Windings of Multi-Speed Wound Rotor Resolvers

Payam MohammadAli Rezayi, Farid Tootoonchian*

***Abstract*—** High efficiency Permanent Magnet (PM) machines are built with high number of poles to meet high power density, and low torque ripple requirements. Their efficient electronic commutation relies on the absolute rotor position. Therefore, the pole number of resolver must equal the pole number of PM. Achieving multi-speed performance using traditional winding configurations needs high number of slots. For the limited outer diameter and the size of the sensor, increasing the number of slots is limited by the mechanical strength of teeth. Therefore, Fractional-Slot Concentrated Winding (FSCW) is proposed for multi-speed resolvers. However, FSCWs suffer from sub-harmonics which cause high position error. To suppress the sub-harmonics, multi-layer winding configuration is employed. Increasing the number of winding layers leads to increase the complexity of the mass production, as well as increasing the possibility of windings faults. In this paper, a new technique based on using flux barriers in the stator core is proposed. Three different shapes are presented for the barriers. The performance of sensor equipped by 2-layer and 4-layer FSCWs, with and without barriers in the stator core, are evaluated using finite-element method. Finally, three prototypes are built and tested and the results verify the performance of the proposed techniques.

***Index Terms*— Finite Element Method (FEM), Magnetic Flux Barrier, Harmonic Content, Tooth-Concentrated Winding, Multi-Speed Resolver**

I. INTRODUCTION

Position transducers are critical part of motion control systems in a variety of industries [1]. Traditionally, position sensors consist of potentiometers, brushed encoders, and magnetic encoders. Due to the higher maintenance requirements, limited resolution, lower reliability, and larger size, these devices are not widely used [2]. Optical encoders and resolvers are becoming increasingly popular due to semiconductor technology developments. In common applications, optical encoders are much more worthwhile and offer sufficient precision [3]. However, resolvers are considered as the primary option in hard conditions where the sensor is subject to wide temperature fluctuation, high shocks and vibrations [4]-[5]. Also, the sensor is exposed to radiation, oil, grease, mist, and dust contaminations [6].

Payam MohammadAli Rezayi is with Electrical Engineering Department, Sharif University of Technology, Tehran, Iran, (e-mail: payamrezayi@ymail.com).

* Farid Tootoonchian (corresponding author) is with the Electrical Engineering Department, Iran University of Science and Technology, Tehran, Iran, (e-mail: tootoonchian@iust.ac.ir). 09121792802

The resolver can be described as a two-phase synchronous generator whose rotor is excited by a high-frequency AC voltage [7]. A resolver has laminated rotors and stators, much like an electrical machine. In the general structure, one winding is located on the rotor and two windings are located on the stator. It is however possible to have more accurate resolver by adding a short-circuited winding to the rotor lamination [8]-[9]. There is an electrical 90° phase difference between the rotor and the stator windings. As a result of applying an AC voltage to the excitation winding of the rotor, quadratic voltages are induced in the stator windings. The amplitude of the induced voltages is determined by the relative position of the rotor and the stator windings. Essentially, the purpose of a resolver is to resolve a vector to its sine and cosine components. With the rotation of the rotor, the induced voltage in the stator windings changes as sine and cosine of the relative position of the rotor changes. The tangent of the shaft position is equal to the division of the voltage of the stator windings.

Similar to the classification of optical encoders into absolute and incremental kinds, resolvers can be categorized into single- and multi-speed categories [10]. In a single-speed, absolute, resolver, an electrical cycle of output voltage corresponds to each 360° mechanical rotation of the shaft. Thus, single-speed resolvers give absolute position of the shaft. However, in multi-speed resolvers, the resolver is wound so that multiple complete sine/cosine waves are produced in a full mechanical rotation of the rotor. In this system, mechanical error sources are minimized due to the higher number of electrical cycles in each mechanical rotation [11]. For high pole number resolvers, mechanical and electromagnetic considerations lead the machine designers to select small cores with a low slot number. Without increasing the number of slots, to achieve high pole number, fractional slot concentrated winding (FSCW) has been proposed by authors of [12] for wound rotor (WR) resolvers.

The influence of integral and fractional slot windings on the accuracy of WR resolvers is discussed in [13]. Results in [12]-[13], demonstrates that FSCW provides the improvements like shorter and less complicated end windings, higher filling factors of slots, better fault tolerance, and lower cost manufacturing process. However, that type of winding contains more magnetic field space harmonics, including subharmonics that are one of the main reasons for inaccuracies in a resolver [12].

To suppress those undesirable harmonics different techniques are proposed by literature. In [14] to overcome the high amplitude of the subharmonics, the excitation winding is designed for 24-pole while the signal windings are designed to peak up the 20-pole flux. Therefore, a 20-pole, 6-layer FSCW resolver with high accuracy is suggested by [14]. Then, the same authors used genetic algorithm in [15] to minimize the total number of coils, the cost of manufacturing process, and complexity of the winding process, as well as increasing accuracy for a disk type WR resolver equipped with FSCW. The main contributions of [14] – [15] for suppressing the sub-harmonics are using multi-layer winding configuration with an optimal shifting angle between layers and the proper slot-pole combination. Authors of [16] suggested an index to compare the quality of FSCW for different slot-pole combinations.

In [17] an innovative multi-stage ferromagnetic core is proposed for the multi-speed resolvers. In the proposed core the slots have a special double-stage shape which allows adjusting the shift of the layers with higher degree of freedom. Finally, in [18] a slot-less configuration is proposed to allow continuous adjustment of the shift angle between layers. Authors of [19] proposed an innovative idea to suppress the high order harmonic content resulted from winding. They developed fractional-slot sinusoidal distributed winding configuration which also benefits from simple structure and convenient mass production. However, that configuration is presented for axial flux variable reluctance resolver and suffer from different number of turns for each coil.

Based on the best knowledge of the authors all the mentioned literature about constant turn windings is focused on using multi-layer configuration with optimal shifting between layers. There is no research on optimal stator core design to achieve reduced sub-harmonics and increase the accuracy of the sensor. Therefore, the contribution of this paper can be mentioned as:

- Using flux barrier in the stator core to suppress undesirable harmonics.
- Examining three different shapes for the flux barriers
- Allocating the appropriate location for the barriers
- Investigating the influence of FSCW's number of layers on effectiveness of different shapes of barriers
- Using constant turn concentrated coils for convenient mass production
- The simulations are done using time stepping finite element method and finally three prototypes of the sensor with the highest accuracy are built and selected for experimental verification.

II. CONVENTIONAL 12-TOOTH/10-POLE WINDING TOPOLOGY

The studied multi-speed (10-pole) resolver with 12 stator teeth and 20 rotor teeth is shown in the Fig. 1. The stator has 2-layer FSCW. The layout of the stator and the rotor windings are shown in Fig. 2-a, and Fig. 2–b, respectively.

The field winding is fed by a $V = 5\sqrt{2}$ V, $f = 4kHz$ sinusoidal voltage. Therefore, for $\omega_f = 2\pi f$, the field voltage can be written as:

$$v_f = V\cos(\omega_f t) = r_f i_f + \frac{d\lambda_f}{dt} \qquad (1)$$

Where r_f denotes the resistance of the field winding, and i_f the field current. The flux linkage of the field winding (λ_f), can be calculated as:

$$\lambda_f = L_f i_f + L_{af} i_a + L_{bf} i_b \qquad (2)$$

Where L_f is self-inductance of the field winding, L_{af} and L_{bf} are the mutual inductance between the field and the stator's a, and b windings. Since the stator winding is connected to the high input impedance Resolver to Digital Converter (RDC), the stator currents, i_a and i_b, are almost zero. Therefore, the field current can be determined as:

$$i_f = \frac{V}{\sqrt{r_f^2 + (\omega_f L_f)^2}} \cos(\omega_f t - \tan^{-1}\frac{\omega_f L_f}{r_f}) = I_f \cos(\omega_f t - \xi) \quad (3)$$

The voltage equations for the stator windings can be written as:

$$v_a = r_s i_a + \frac{d\lambda_a}{dt} \quad (4)$$

$$v_b = r_s i_b + \frac{d\lambda_b}{dt} \quad (5)$$

Where v_a and v_b are phase voltages, r_s is resistance of the signal winding, λ_a and λ_b are flux linkage of the stator's orthogonal windings and can be written as:

$$\lambda_a = L_a i_a + L_{af} i_f = L_{af} i_f = L\sin(\alpha) i_f \quad (6)$$

$$\lambda_b = L_b i_b + L_{bf} i_f = L_{bf} i_f = L\cos(\alpha) i_f \quad (7)$$

Where L denotes the peak value of the stator-to-rotor mutual inductance and α the rotor angle. Substituting Eq. (6) - Eq. (7) into Eq. (4) – Eq. (5) leads to:

$$v_a = \frac{d}{dt}(L\sin(\alpha) i_f) = L i_f \cos(\alpha)\omega_m + L\sin(\alpha)\frac{di_f}{dt} \quad (7)$$

$$v_b = \frac{d}{dt}(L\cos(\alpha) i_f) = -L i_f \sin(\alpha)\omega_m + L\cos(\alpha)\frac{di_f}{dt} \quad (8)$$

Where $\omega_m = \frac{d\alpha}{dt}$ denotes the mechanical speed of the rotor. Then, substituting Eq. (3) into Eq. (4) – Eq. (5), leads to:

$$v_a = L I_f \omega_f \left\{ \frac{\omega_m}{\omega_f} \cos(\alpha)\cos(\omega_f t - \xi) + \sin(\alpha)\sin(\omega_f t - \xi) \right\} \quad (9)$$

$$v_b = -L I_f \omega_f \left\{ \frac{\omega_m}{\omega_f} \sin(\alpha)\cos(\omega_f t - \xi) + \cos(\alpha)\sin(\omega_f t - \xi) \right\} \quad (10)$$

Since $\omega_m \ll \omega_f$, the first term in Eq. (4) – Eq. (5) is almost equal to zero. Therefore, the induced voltages in the stator windings, as shown in Fig. 3-a, are amplitude modulated (AM) signals, as:

$$v_a = L I_f \omega_f \sin(\alpha)\sin(\omega_f t - \xi) \quad (11)$$

$$v_b = -LI_f \omega_f \cos(\alpha)\sin(\omega_f t - \xi) \qquad (12)$$

Peak detection method is used to determine the envelope of the signals. Total Harmonic Distortion (THD) of the envelopes is 2.296% and the amplitude of the fundamental harmonic of the envelopes is 1.5798 V. Then, inverse tangent of the division of the envelopes' is used to calculate the rotor position (Fig. 3-b).

Comparing the calculated position with the reference position leads to position error, as given in Fig. 3-c. Maximum Position Error (MPE) of the studied sensor is 0.280 ° and the Peak to Peak value of the Position Error (PPPE) is equal to 0.559 °. However, the best index for evaluating the performance of a resolver is Average of Absolute Position Error (AAPE) that its value is 0.170 ° for the studied resolver.

The calculated values of THD and AAPE are higher than expected values for a 10-pole WR resolver. To determine the reason, the air gap flux density and its corresponding space harmonics are presented in Fig. 4-a, and 4–b, respectively. For plotting the distribution of Fig. 4-a, the excitation and the cosine windings are opened and the sine winding is supplied by a DC current. The same Fig. with the 90˚ phase shift can be plotted for the cosine winding. That distribution shows the location of the magnetic flux barriers in the stator yoke. Based on the calculated distributions, the flux barriers should be created on the both sides of teeth #2, and #8 and considering the distribution for the cosine winding, the barriers should be on both sides of teeth #5, and #11. The Fig. 4-b illustrates that among the dominant space harmonics for the employed 2-layer FSCW, the first, third, fifth, seventh, ninth, 17th, and 19th are the most prominent. Nevertheless, only the fifth harmonic of the stator interacts with the rotor field in the 10-pole resolver. The remaining space harmonics, especially the 1st, 3rd, 7th, 17th, and 19th, which have relatively large magnitudes, are undesirable harmonics that may restrict the applicability of the employed FSCW.

An idea to improve the performance of the studied resolver is using an optimal 4-layer winding on the stator. The winding layout of the 4-layer FSCW is given in Fig. 5. The induced voltages in the signal windings, the envelope of the voltages, the calculated position and the position error of the sensor with 4-layer FSCW are given in Figs. 6–a, through 6-c, respectively. Using 4-layer winding, the THD of envelopes reduced to 0.140% and the amplitude of the fundamental harmonic increased to 2.735 V. MPE, PPPE and the AAPE have a significant improvement and their value is equal to 0.022 ˚, 0.043 ˚, and 0.008 ˚, respectively. Although, using 4-layer winding significantly improves the accuracy of the studied resolver, it leads to higher manufacturing difficulties and possibility of winding errors in the manufacturing process. Therefore, in the following using different shapes of the flux barriers in the stator core are examined to achieve higher accuracy of the studied resolver.

III. FLUX BARRIERS IN STATOR YOKE

As mentioned previously, it is possible to reduce the sub-harmonics for the tooth concentrated windings by using magnetic flux barriers in the stator yoke. In order to realize the new stator core with flux barriers in the stator yoke, the structure of the stator

yoke can be modified in various ways, including using holes of different shapes, and slot depths, or completely dividing the stator yoke into specific rentals [20]. Figs. 7-a through 7-c show the different shapes of the stator core equipped with the flux barriers. In Fig. 7-a, the circle shape flux barrier is used in the stator core. That configuration is so-called the 1st structure. In the 2nd structure, as shown in Fig. 7-b, the stator yoke is divided into individual parts and in the 3rd structure, Fig. 7-c, the deep slot shape is considered in the stator core.

Distribution of the flux density in the middle of the air-gap length and its harmonic content for the studied configurations are given in Figs. 8-a, and 8-b, respectively. It is worth mentioning that the amplitude of the magnetic flux density in the middle of the air-gap length for different configurations is normalized based on the amplitude of that for the conventional core with 2-layer winding. Also, the amplitude of the fundamental harmonic for 2-layer winding with conventional core is considered as the base of normalization of harmonic content for all different configurations. As it can be seen in Fig. 8-b, conventional core with 4-layer FSCW has the highest amplitude for the 5th harmonic (fundamental harmonic). The ratio of the 1st, 7th, 11th, 17th, and 19th harmonics to the fundamental for 2-layer winding with conventional core is equal to that of 4-layer winding. However, the 3rd, 9th, and 15th harmonics are almost canceled using the 4-layer winding. Among 2-layer windings with different structure of cores, the 2nd structure has the lowest harmonic content for the equal fundamental amplitude. Therefore, the 2nd structure is expected to have the highest accuracy among 2-layer windings.

The induced voltages in the 2-layer FSCW of the stator for different structures are given in Fig. 9-a, through 9-c and the position error of those studied configurations, as well as that of conventional core with 2- and 4-layer winding is presented in Fig. 9-d.

The induced voltages in the 2-layer FSCW of the stator for different structures are given in Fig. 9-a, through 9-c and the position error of those studied configurations, as well as that of conventional core with 2- and 4-layer winding is presented in Fig. 9-d.

As it was predictable, refereeing to Fig. 9-d, the highest accuracy is achieved using conventional core with 4-layer winding. Among different structures equipped with 2-layer winding, the 2nd one with discrete stator core has the best performance. AAPE for the 1st, 2nd and the 3rd structure is equal to 0.168 ˚, 0.067 ˚, and 0.168 ˚, respectively. Also, their PPPE is equal to 0.553˚, 0.237˚, and 0.557˚, respectively.

Comparing the position error of the studied resolvers results into a question, “is it possible to further improve the performance of 12-tooth, 10-pole WR resolver by using flux barriers in the core of 4-layer FSCW resolver?” To answer it, all the studied structures are equipped with 4-layer FSCW and re-designed for appropriate flux barrier location. The induced voltages and the position error of those structures are presented in Fig. 10.

The performance characteristic of the different structures is summarized in Table I. From THD of the envelopes point of view, the best performance is related to the 4-layer winding with the first structure of the core. However, the highest amplitude of the fundamental harmonic of the envelopes is referred to the 4-layer winding with conventional core. Considering the MPE as the accuracy index, the 4-layer winding with conventional core and the 3rd structure of the core have the lowest value of MPE. While, considering peak to peak value of the position error the best accuracy is devoted to the 4-layer winding with conventional core. Finally, based on the AAPE, as the most reliable accuracy index of a sensor, 4-layer winding with the first or the third structures has the lowest position error. The accuracy improvement in Table I is calculated based on the variation of the AAPE of different configurations with respect to that of 2-layer and 4-layer FSCW with conventional core. It can be seen, adding different shapes of flux barriers in 2-layer winding leads to accuracy improvement and using discrete core is the best configuration for the 2-layer winding. However, using 4-layer winding significantly improves the accuracy and adding flux barriers has no significant change in the accuracy of 4-layer winding. Therefore, considering the highest accuracy improvement, the 3rd structure with the 4-layer winding is the best configuration for the studied 5-X resolver. However, taking both the accuracy and the simplicity of practical implementation into account 2-layer winding with the 2nd structure of the core can be a good choice.

IV. Experimental Measurements

In order to verify the obtained results, three prototypes are built and tested. The first prototype has 2-layer winding with conventional core, the second one has 2-layer winding with the 2nd structure of the core and the 3rd prototype is the conventional core with 4-layer winding.

Figs. 11-a, and 11-b show the rotor and the conventional stator cores, respectively. The conventional stator core after winding is shown in Fig. 11-c, and the discrete stator core (2nd structure) is given in Fig. 11-d.

The test setup of the resolvers is given in Fig. 12-a where a DC motor is used for rotating the rotor of the sensors with a constant speed. An optical encoder is mechanically coupled to the shaft of the motor to be used as the sensor of the reference position. The excitation winding of the prototypes is fed through a rotary transformer whose primary winding is supplied from a digitally synthesized function generator with the resolution of 0.1 Hz and the amplitude of excitation voltage is adjusted using an automatic gain control (AGC) circuit. The block diagram of the test circuit is given in Fig. 12-b. The signal voltages, as presented in Figs.13-a through 13-c, are saved using a digital oscilloscope in logging mode with the sampling rate of 1 GS/sec and imported to the MATLAB software. The high frequency content of the measured amplitude modulated voltages are extracted and the inverse tangent method is used to calculate the measured position. Then, the position error of the prototypes is calculated by comparing the measured position by prototypes and that of optical encoder. Also, repeatability of the prototypes is examined by repeating the experimental test for 10 times. The results of different measurements were very close to each other. The average position error of

ten measurements is presented as the experimental result to ensure considering the uncertainty of the experimental test. Fig. 13-d shows the AAPE of the prototypes versus that of the simulations. It is shown that test results confirm the simulation results.

V. CONCLUSION

In this paper, the influence of using magnetic flux barriers in the stator yoke of a 12-teeth/10-poles, 2-layer and 4-layer FSCW wound resolver was studied. Using flux barriers in the stator yoke reduces the subharmonics of the air gap flux density in electrical machines with concentrated windings. It was shown the shape of the flux barrier could influence the accuracy of the sensor. Also, the optimal shape for 2-layer and 4-layer windings were different. Considering 2-layer winding, the best improvement was achieved using discrete shape of the core, called 2nd structure, with 60.588% accuracy improvement. While that structure with 4-layer winding has no success for reduction of AAPE. Furthermore, the highest accuracy improvement, 95.882%, was achieved using the 1st and the 3rd structure with 4-layer winding. The measured and the simulation results approved that using 4-layer winding with the conventional core was more successful than the modified cores with 2-layer winding in accuracy enhancement.

VI. REFERENCES

[1] Ghandehari R., Naderi P. and Vandevelde L. “Performance analysis of a new type PM-resolver in healthy and eccentric cases by an improved parametric MEC method”, *IEEE Transactions on Instrumentation and Measurement*, **70**, pp. 1-10 (2021). DOI: 10.1109/TIM.2021.3080388

[2] KhajueeZadeh M., Zare F. and Nasiri-Gheidari Z. “Reliability analysis of two resolver configurations under faulty conditions in 2DOF system”, *IEEE Transactions on Instrumentation and Measurement*, **72**, pp. 1-8 (2023). DOI: 10.1109/TIM.2022.3229711

[3] Bahari, M., & Nasiri-Gheidari, Z. “The comparative analysis of AC- flux and DC-flux resolvers”, *Scientia Iranica*, **29**(4), pp. 2007-2013 (2022). DOI:10.24200/sci.2019.52439.2764

[4] Mohammad-Yari, M., Safari, M. R., Alipour-Sarabi, R., et al. “Optimal winding selection for wound-rotor resolvers”, *Scientia Iranica*, **28**(6), pp. 3429-3436 (2021). DOI: 10.24200/sci.2019.52439.2764

[5] Saneie H., Nasiri-Gheidari Z. and Belahcen A. “On the field-reconstruction method for electromagnetic modeling of resolvers”, *IEEE Transactions on Instrumentation and Measurement*, **72**, pp. 1-8 (2023). DOI: 10.1109/TIM.2022.3224527

[6] Naderi P. and Ghandehari R. "Comprehensive analysis on a new type VR-resolver with toroidal windings under healthy and eccentric cases”, *IEEE Transactions on Industrial Electronics*, **69**(12), pp. 13754 – 13762 (2022). DOI: 10.1109/TIE.2021.3130318

[7] Naderi P., Sharouni S. and Ehsan-Maleki B. "A novel robust linear resolver proposal and performance analysis under healthy and air-gap asymmetry fault", *IEEE Transactions on Instrumentation and Measurement*, **72**, pp. 1-8 (2023). OI: 10.1109/TIM.2023.3322480

[8] Lasjerdi H. and, Nasiri-Gheidari Z. "Improving the performance of variable reluctance resolver against short circuit using physical parameters", *Scientia Iranica* (2023). DOI: 10.24200/sci.2023.62539.7901

[9] Hajmohammadi S., Alipour-Sarabi R., Nasiri-Gheidari Z., et al. "Influence of different installation configurations on the position error of a multiturn wound-rotor resolver", *IEEE Sensors Journal*, **20(**11), pp. 5785-5792 (2020). DOI: 10.1109/JSEN.2020.2973225

[10] Hajmohammadi S., Alipour-Sarabi R., Nasiri-Gheidari Z., et al. "Design Cconsiderations of multi-turn wound-rotor resolvers", *2019 10th International Power Electronics, Drive Systems and Technologies Conference (PEDSTC)*, pp. 166-171 (2019). DOI: 10.1109/PEDSTC.2019.8697822

[11] Prentice M. "Resolvers 101: understanding the basics", *Dynapar Industry White Papers*, www.dynapar.com

[12] Alipour-Sarabi R., Nasiri-Gheidari Z., Tootoonchian F., et al. "Analysis of winding configurations and slot-pole combinations in fractional-slots resolvers", *IEEE Sensors Journal*, **17(**14), pp. 4420-4428 (2017). DOI: 10.1109/JSEN.2017.2707523

[13] Onsal M., Demir Y. and Aydin M. "Comparison of fractional and integral slot winding configurations on the position error for a conventional wound-rotor resolver", *IEEE International Magnetic Conference - Short Papers (INTERMAG Short Papers)*, Sendai, Japan, pp. 1-2 (2023). DOI: 10.1109/INTERMAGShortPapers58606.2023.10228498

[14] Alipour-Sarabi R., Nasiri-Gheidari Z., Tootoonchian F., et al. "Performance analysis of concentrated wound-rotor resolver for its applications in high pole number permanent magnet motors", *IEEE Sensors Journal*, **17**(23), pp. 7877-7885 (2017). DOI: 10.1109/JSEN.2017.2761796

[15] Alipour-Sarabi R., Nasiri-Gheidari Z., Tootoonchian, F., et al. "Improved winding proposal for wound rotor resolver using genetic algorithm and winding function approach", *IEEE Transactions on Industrial Electronics*, **66**(2), pp. 1325-1334 (2019). DOI: 10.1109/TIE.2018.2821091

[16] Hajmohammadi S. and Tootoonchian F. "Simplification of integrated multi-turn wound-rotor resolvers' manufacturing", *IEEE Sensors Journal*, **20**(23), pp. 14141-14147 (2020). DOI: 10.1109/JSEN.2020.3007807

[17] Alemi-Rostami M., Alipour-Sarabi R., Rezazadeh, G. et al. "Design optimization of a double-stage resolver", *IEEE Transactions on Vehicular Technology*, **68**(6), pp. 5407-5415 (2019). DOI: 10.1109/TVT.2019.2909096

[18] Moheyseni A., Nasiri-Gheidari Z. and Alipour-Sarabi R. “slotless disk type resolver: a solution to improve the accuracy of multi-speed wound rotor resolvers”, *IEEE Transactions on Transportation Electrification*, **8**(1), pp. 1493-1500 (2022). DOI: 10.1109/TTE.2021.3111702

[19] Ran X., Shang J., Zhao M., et al. “Improved configuration proposal for axial reluctance resolver using 3-D magnetic equivalent circuit model and winding function approach”, *IEEE Transactions on Transportation Electrification*, **9**(1), pp. 311-321 (2023). DOI: 10.1109/TTE.2022.3199538

[20] Dajaku G., Xie W. and Gerling D. “Reduction of low space harmonics for the fractional slot concentrated windings using a novel stator design”, *IEEE Transactions on Magnetics*, **50**(5), pp. 1-12 (2014). DOI: 10.1109/TMAG.2013.2294754

Fig. 1. The studied 5-X Resolver with the 12 stator teeth and 20 rotor teeth

Fig. 2. The schematic of the 2-layer, FSCWs of the studied resolver: (a) stator winding, and (b) rotor winding

Fig. 3. The finite element simulation of the studied resolver with 2-layer FSCW: (a) the induced voltages and the envelopes, (b) the calculated position, and (c) position error

Fig. 4. 2-Lyer FSCW with conventional core: (a) the distribution of flux density in the middle of the air-gap length and (b) Harmonic content of the air gap flux density

Fig. 5. The 4-layer FSCW layout for the studied resolver (Red: Cosine coils and Green: Sine coils)

Fig. 6. The finite element simulation of the studied resolver with 4-layer FSCW: (a) the induced voltages and the envelopes, (b) the calculated position, and (c) position error

Fig. 7. Using flux barrier in the stator core of studied resolver with 2-layer FSCW: (a) the 1st structure, (b) the 2nd structure, and (c) the 3rd structure

Fig. 8. Comparison of different configurations: (a) the distribution of the flux density in the middle of the air-gap length, and (b) harmonic content of flux density

Fig. 9. The output characteristic of the studied resolver with the proposed structures: (a) signal voltages of 1st structure, (b) signal voltages of 2nd structure, (c) signal voltages of 3rd structure, and (d) position error of all studied configurations

Fig. 10. The output characteristic of the studied resolver with the proposed structures and 4-layer FSCW: (a) signal voltages of 1st structure, (b) signal voltages of 2nd structure, (c) signal voltages of 3rd structure, and (d) position error of all studied configurations

Fig. 11. The prototyped sensors: (a) the rotor core before winding, (b) the rotor after winding, (c) the conventional stator, and (d) the discrete stator core

Fig. 12. Experimental test: (a) the employed test setup, and (b) the block diagram of the test circuit

Fig. 13. The experimental results: (a) signal voltages of 2-layer winding with conventional core, (b) signal voltages of 2-layer winding with discrete core, (c) signal voltages of 4-layer winding with conventional core, and (d) comparing AAPE of prototypes with the simulation results

Table 1. Performance characteristic of different studied structures for 12-tooth, 10-pole WR resolver

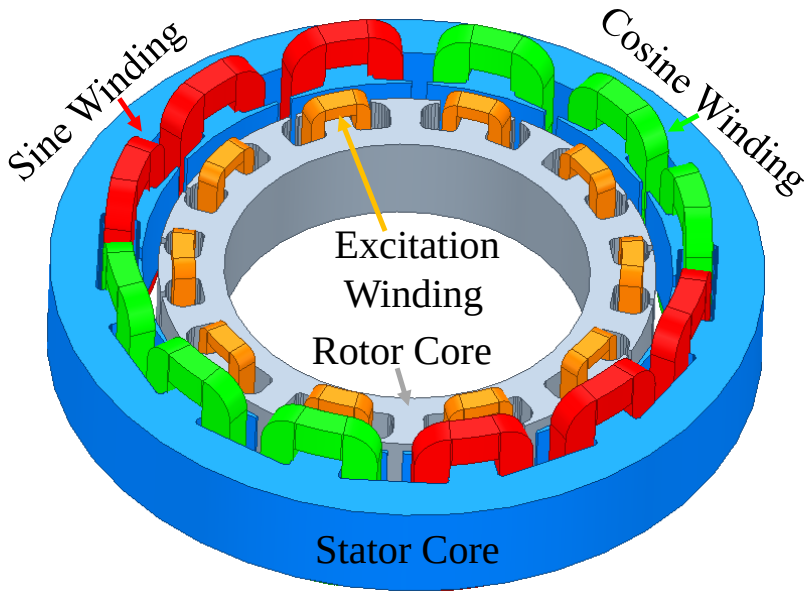

Fig. 1. The studied 5-X Resolver with the 12 stator teeth and 20 rotor teeth

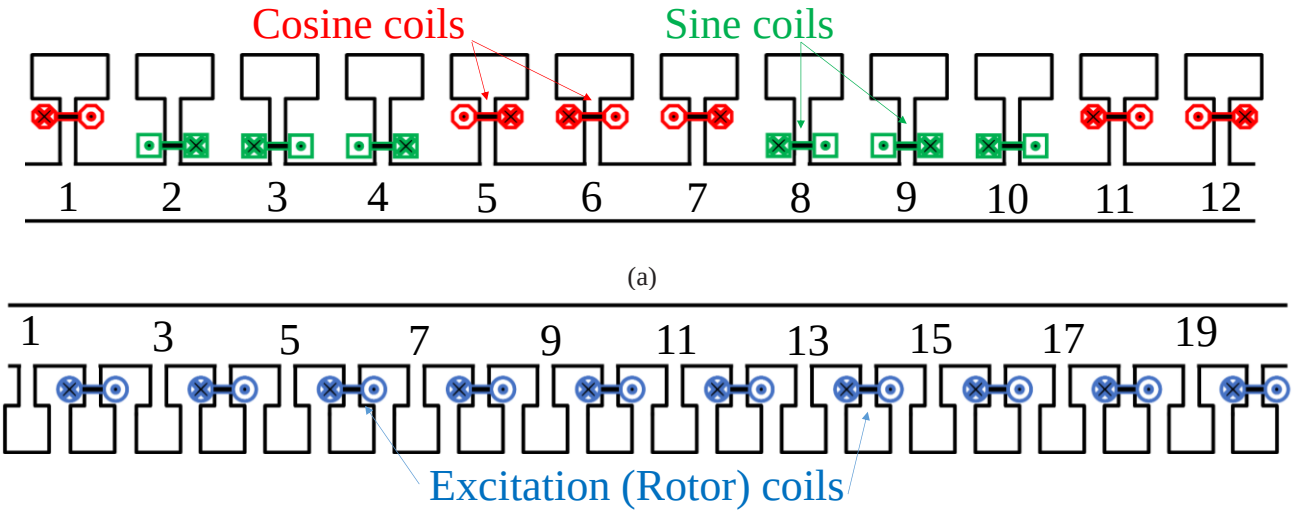

(a)

(b)

Fig. 2. The schematic of the 2-layer, FSCWs of the studied resolver: (a) stator winding, and (b) rotor winding

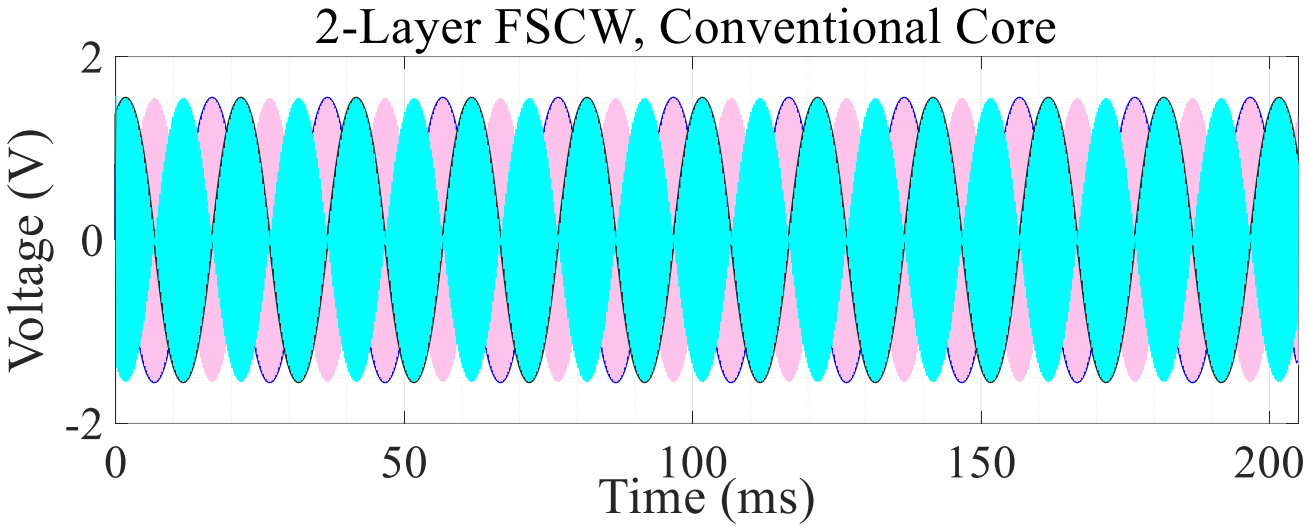

(a)

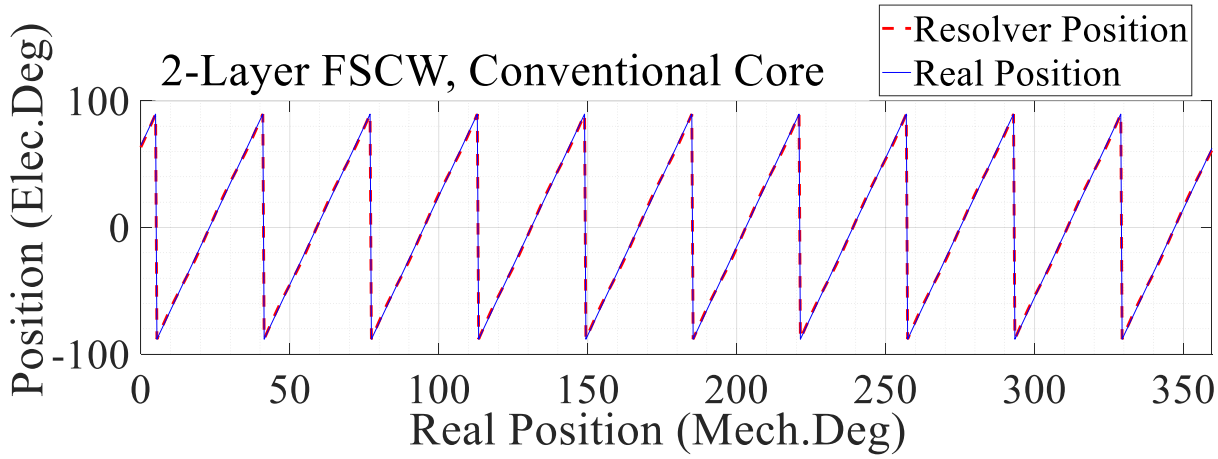

(b)

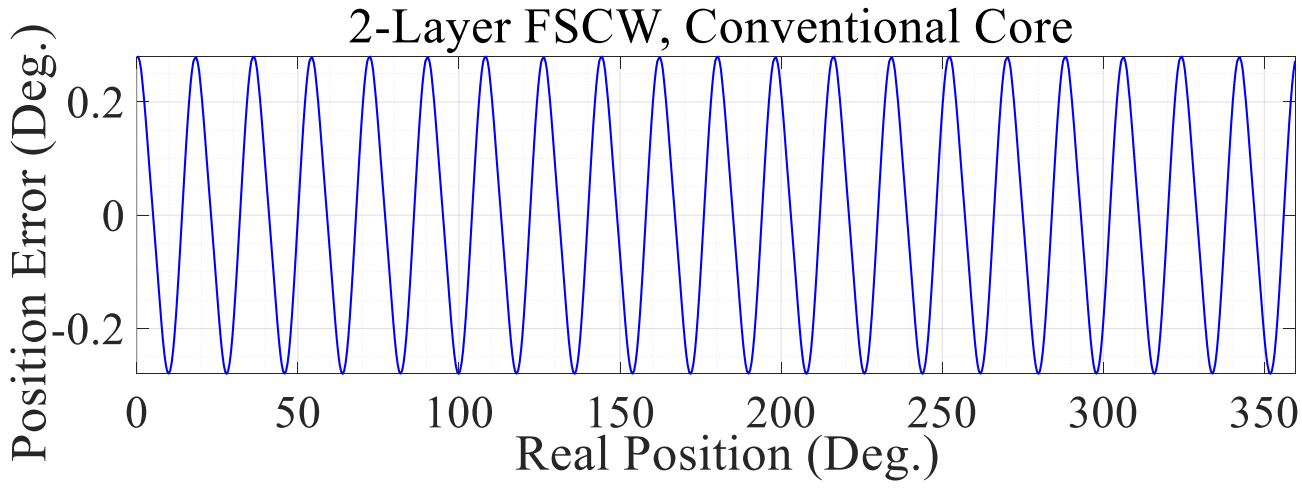

(c)

Fig. 3. The finite element simulation of the studied resolver with 2-layer FSCW: (a) the induced voltages and the envelopes, (b) the calculated position, and (c) position error

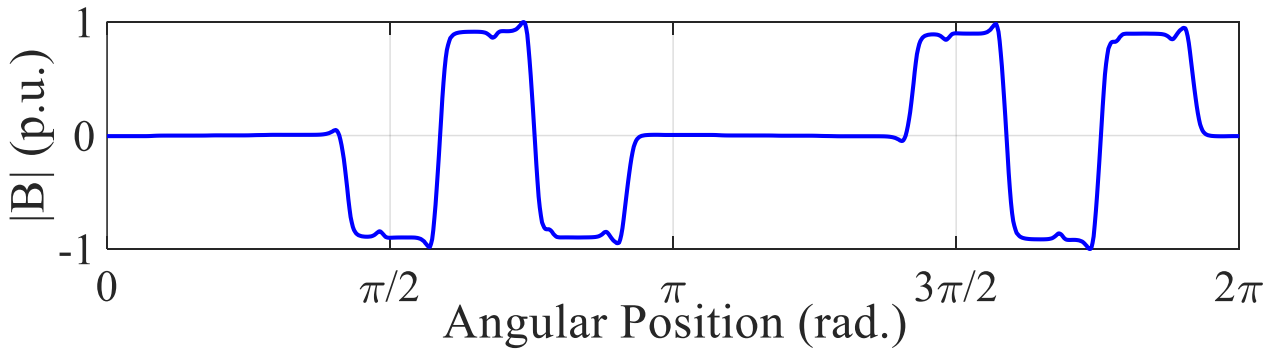

(a)

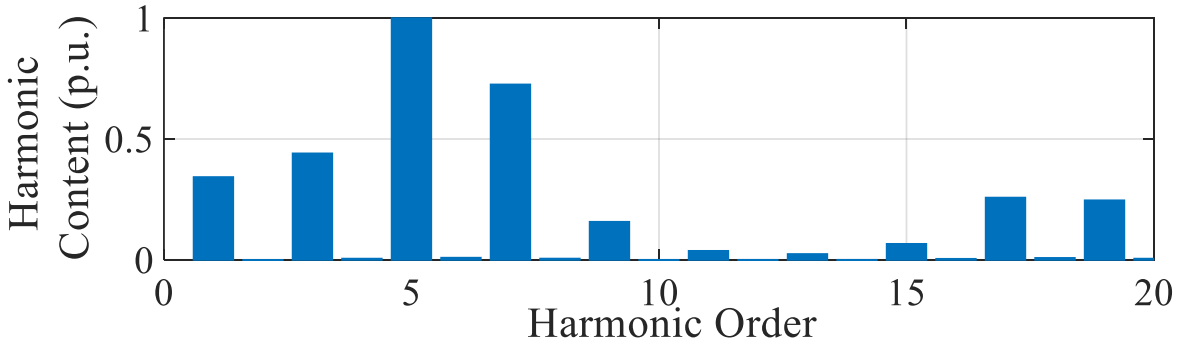

(b)

Fig. 4. 2-Lyer FSCW with conventional core: (a) the distribution of flux density in the middle of the air-gap length and (b) Harmonic content of the air gap flux density

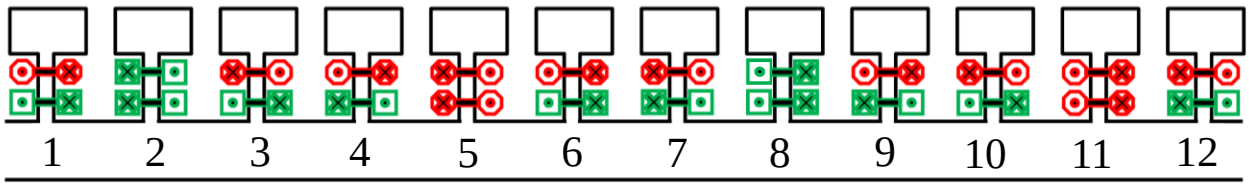

Fig. 5. The 4-layer FSCW layout for the studied resolver (Red: Cosine coils and Green: Sine coils)

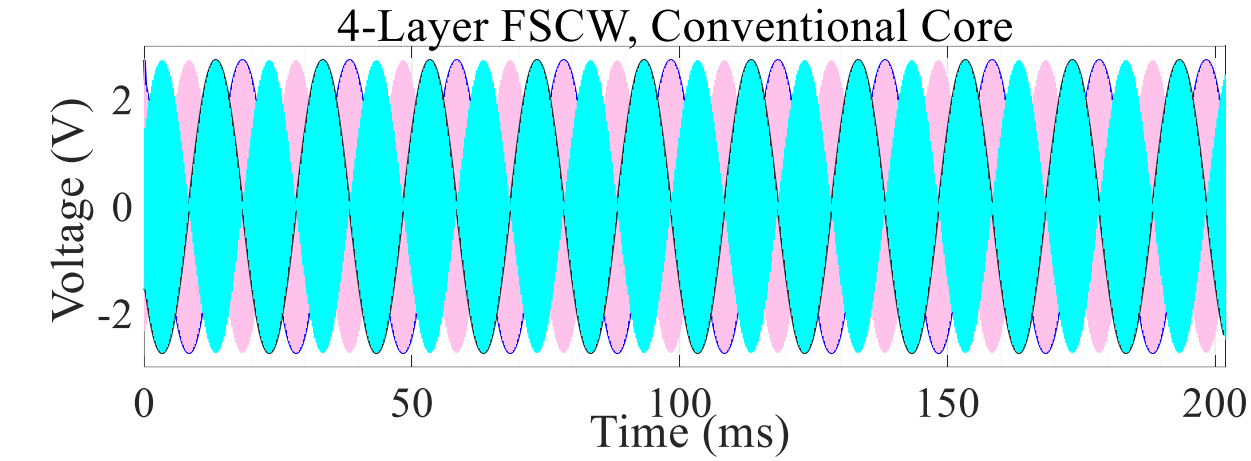

(a)

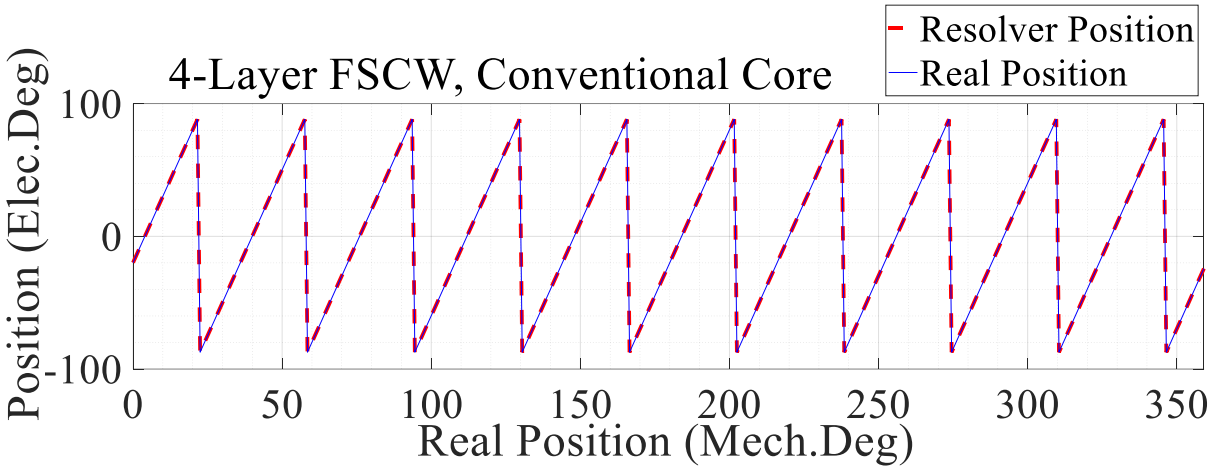

(b)

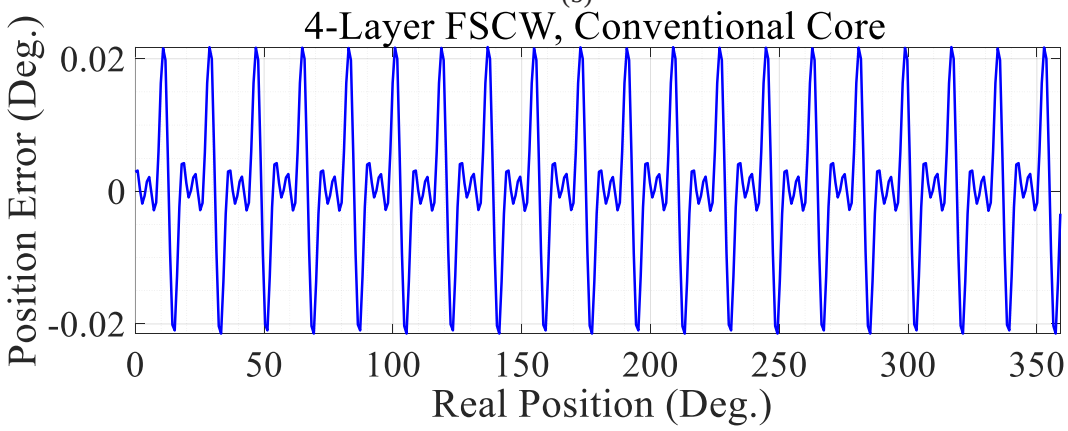

(c)

Fig. 6. The finite element simulation of the studied resolver with 4-layer FSCW: (a) the induced voltages and the envelopes, (b) the calculated position, and (c) position error

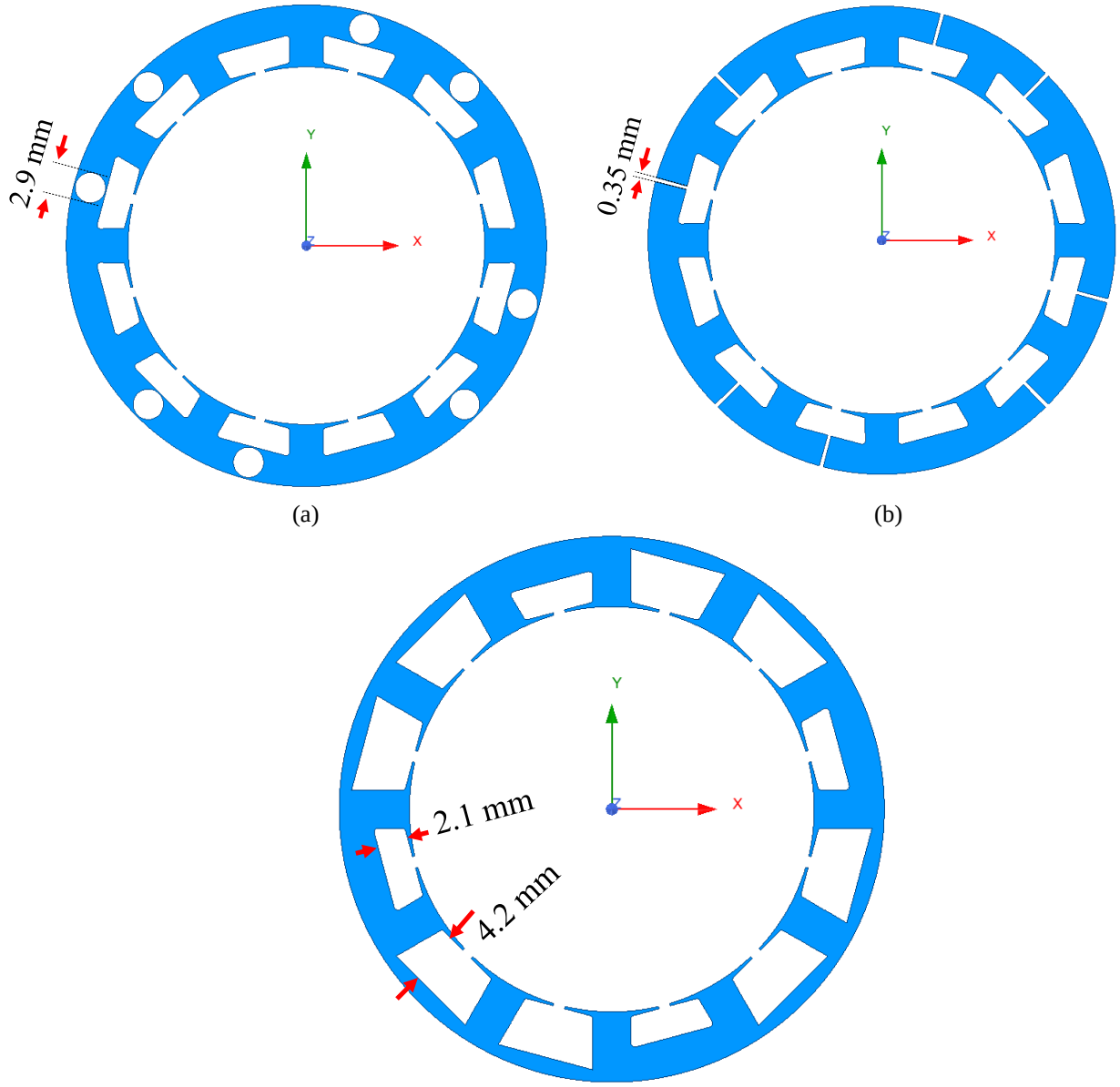

Fig. 7. Using flux barrier in the stator core of studied resolver with 2-layer FSCW: (a) the 1st structure, (b) the 2nd structure, and (c) the 3rd structure

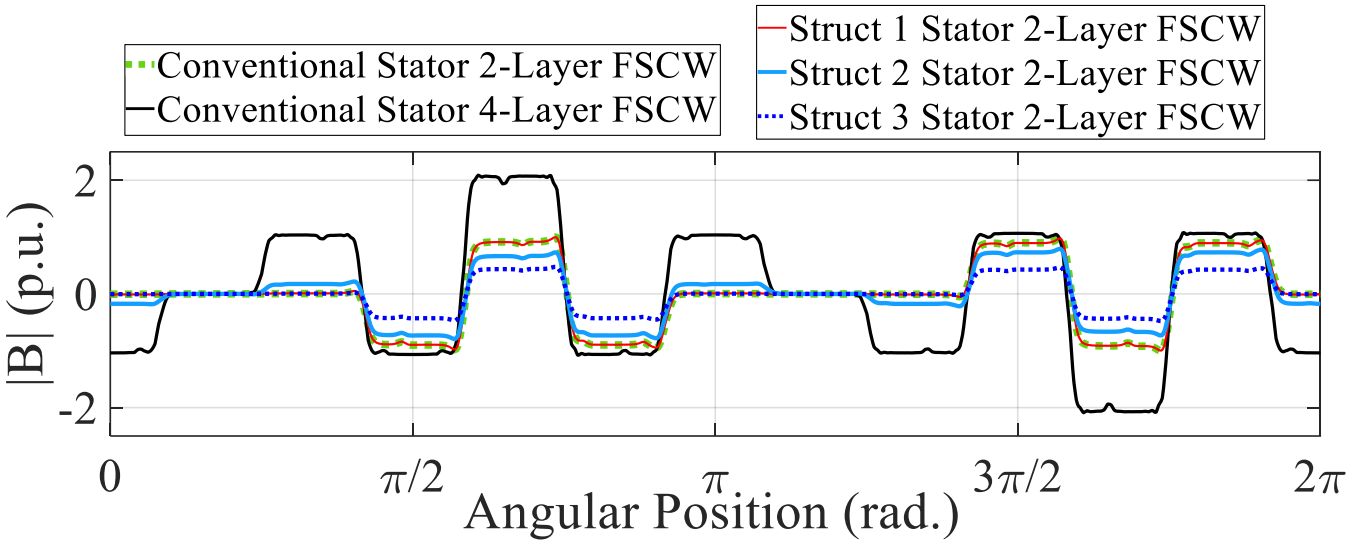

(a)

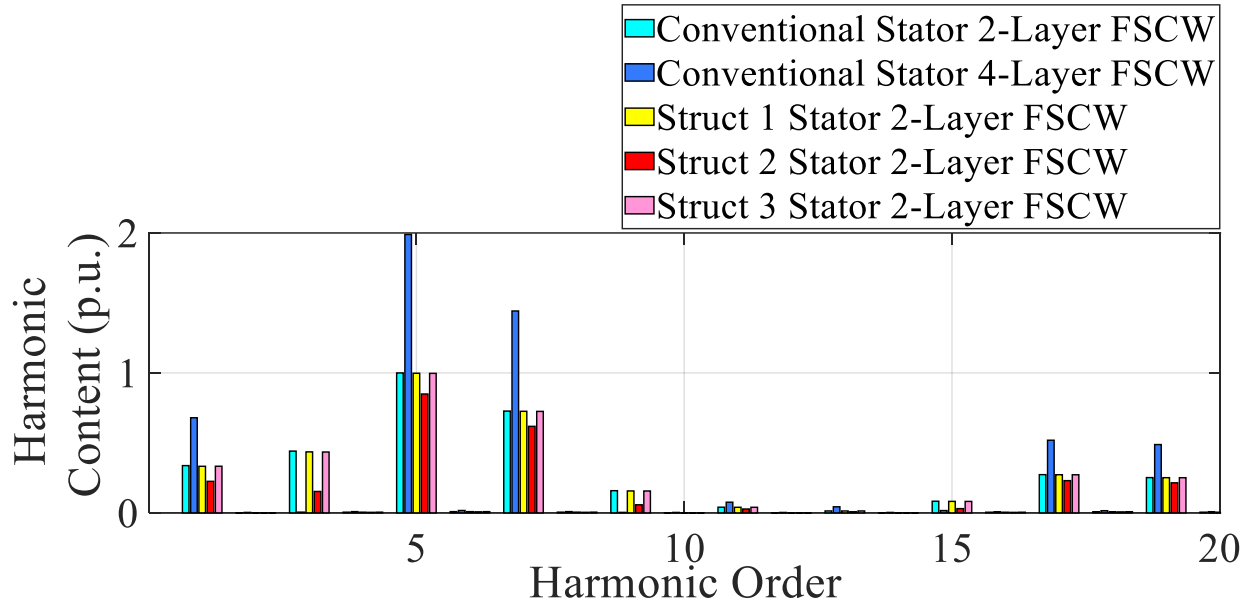

(b)

Fig. 8. Comparison of different configurations: (a) the distribution of the flux density in the middle of the air-gap length, and (b) harmonic content of flux density

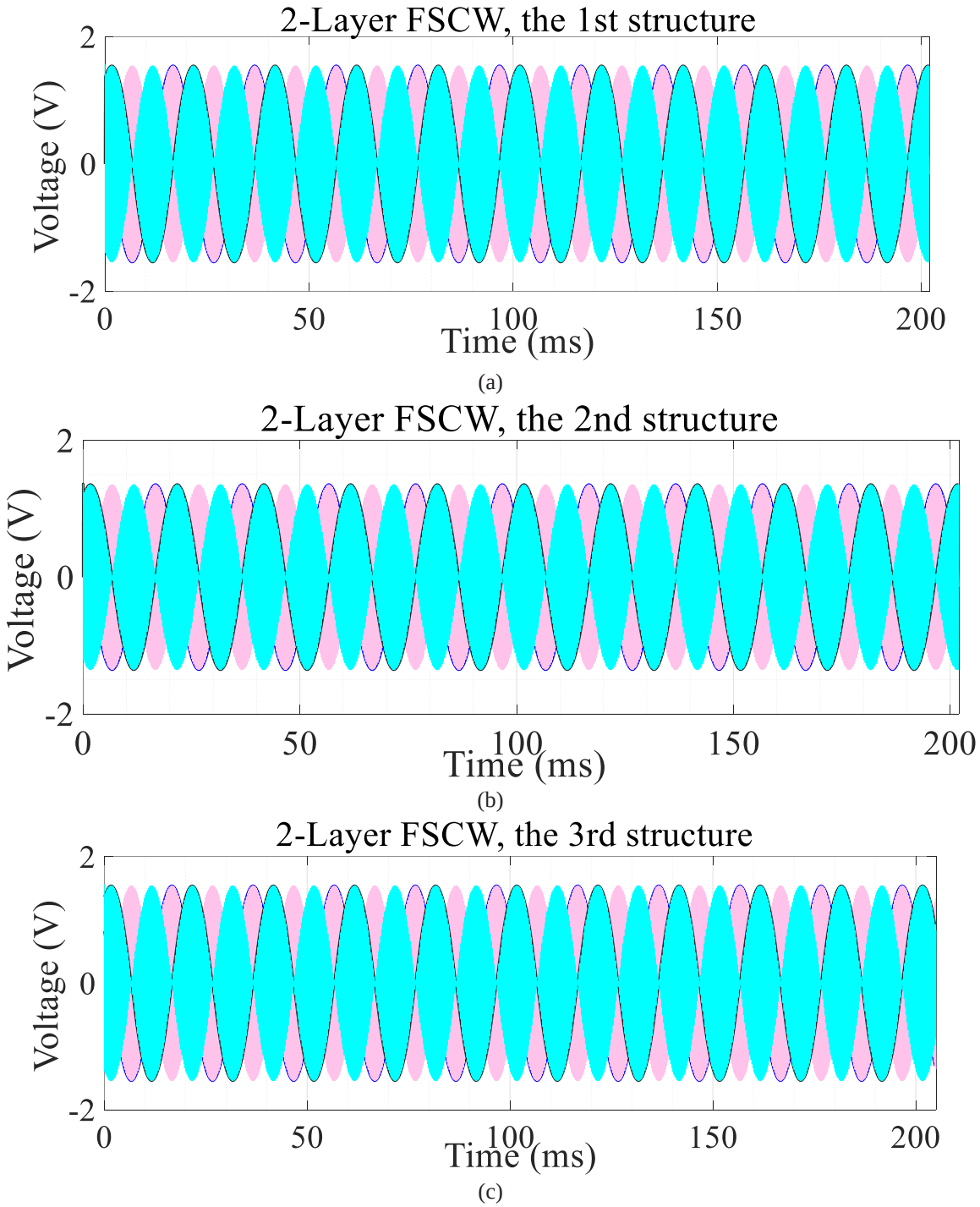
2-Layer FSCW, the 1st structure
Voltage (V)
Time (ms)
(a)
2-Layer FSCW, the 2nd structure
Voltage (V)
Time (ms)
(b)
2-Layer FSCW, the 3rd structure
Voltage (V)
Time (ms)
(c)

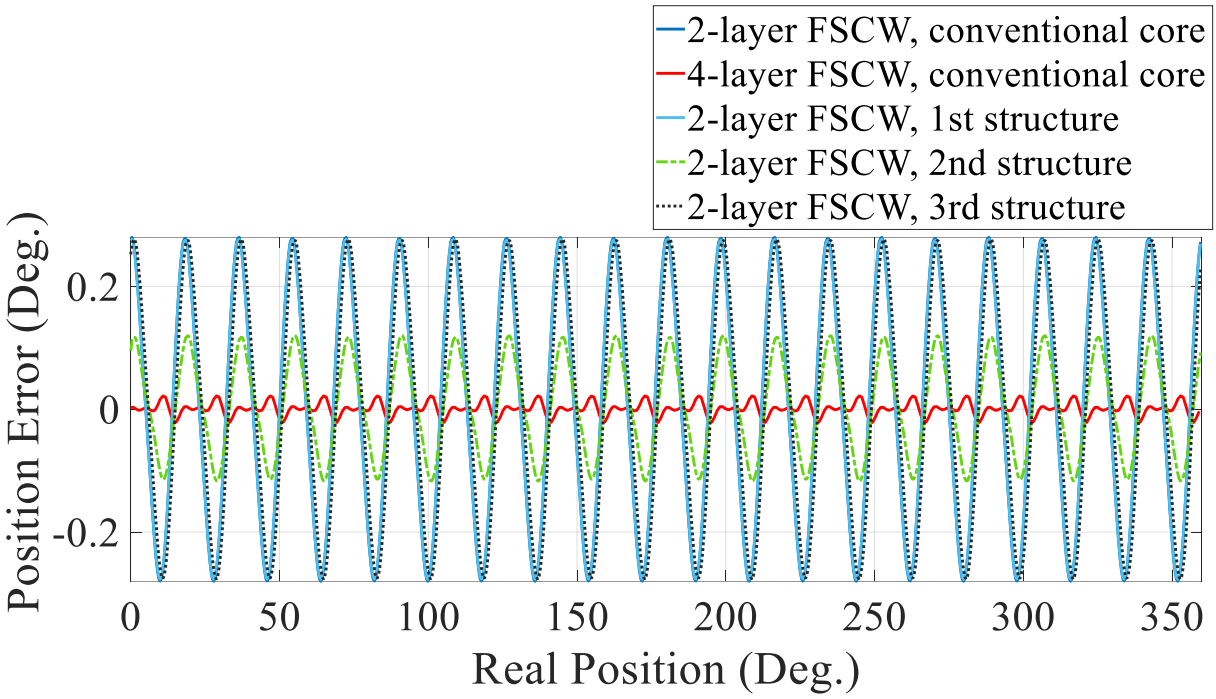

(d)

Fig. 9. The output characteristic of the studied resolver with the proposed structures: (a) signal voltages of 1st structure, (b) signal voltages of 2nd structure, (c) signal voltages of 3rd structure, and (d) position error of all studied configurations

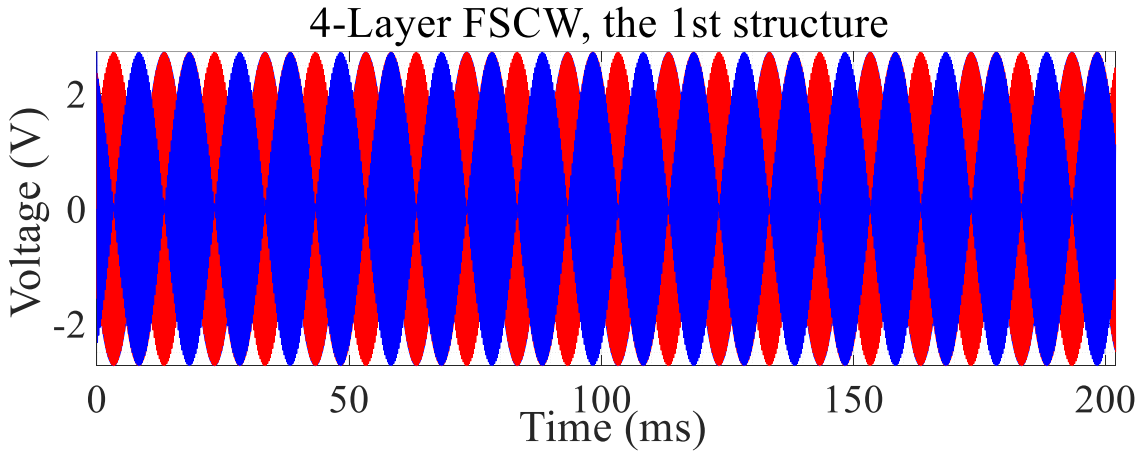

(a)

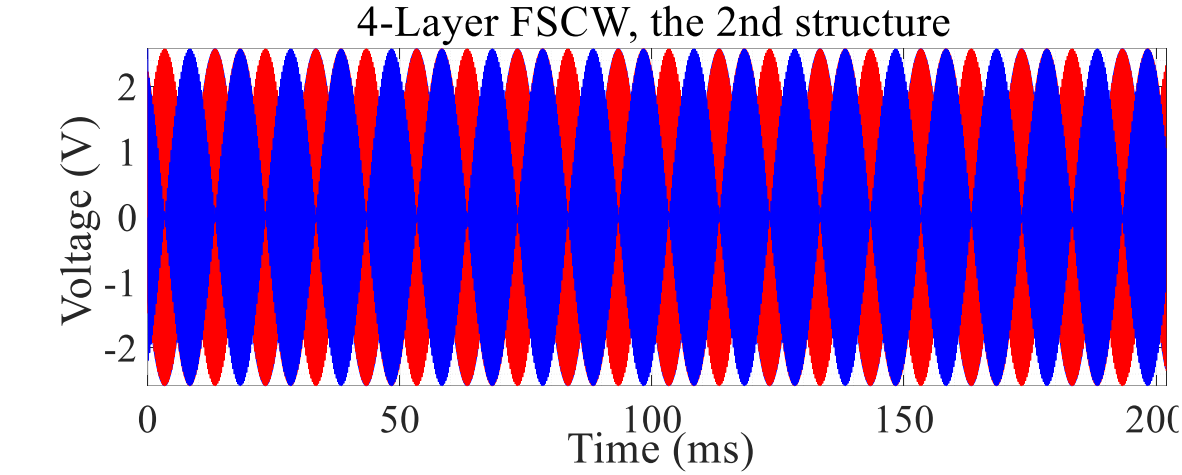

(b)

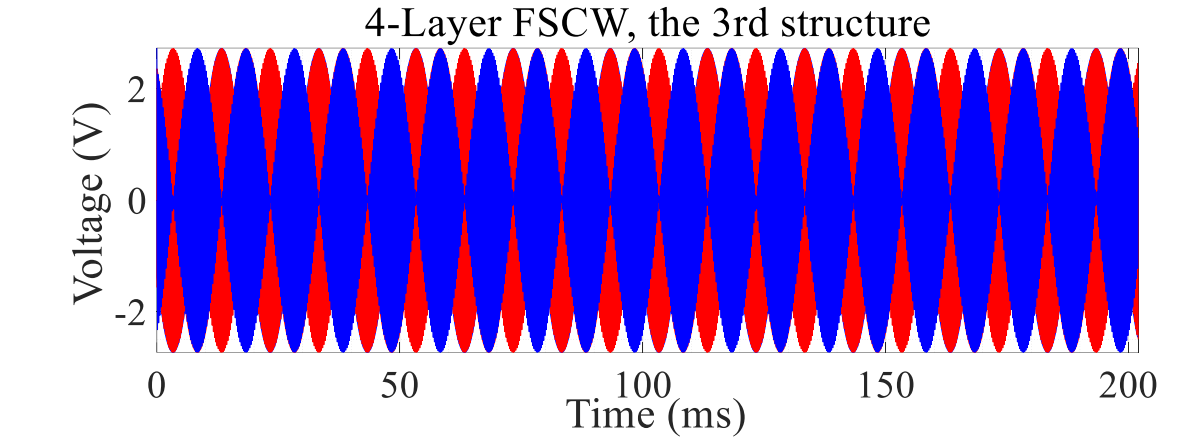

(c)

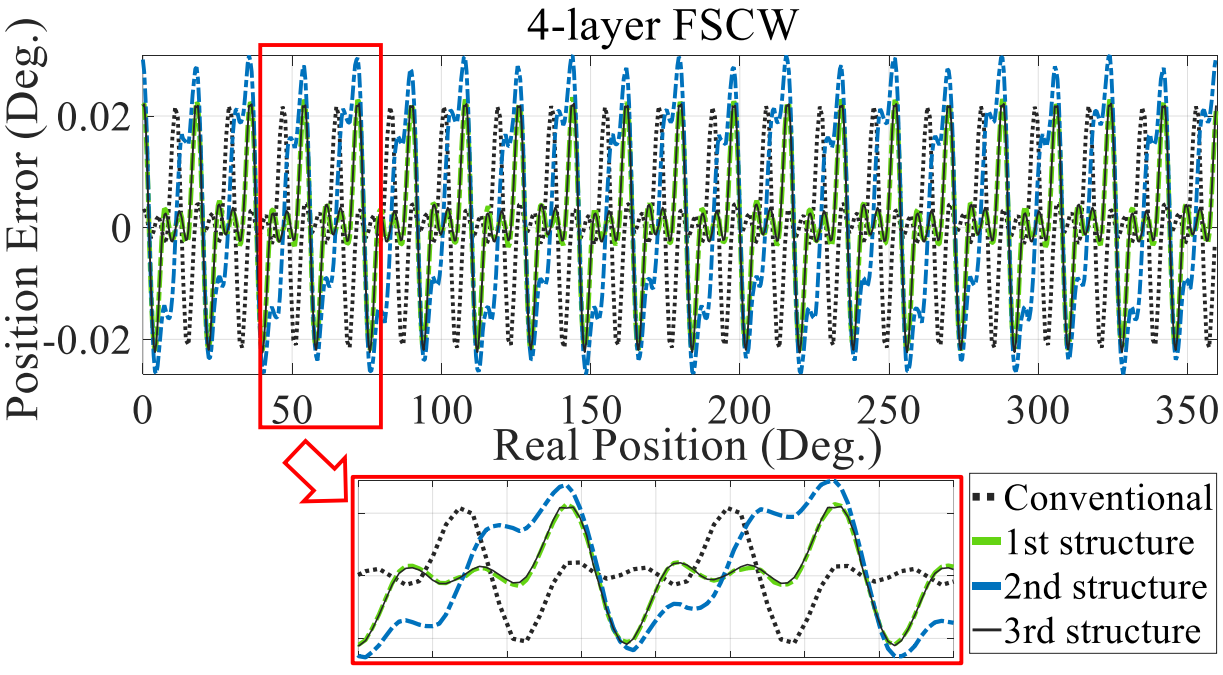

(d)

Fig. 10. The output characteristic of the studied resolver with the proposed structures and 4-layer FSCW: (a) signal voltages of 1st structure, (b) signal voltages of 2nd structure, (c) signal voltages of 3rd structure, and (d) position error of all studied configurations

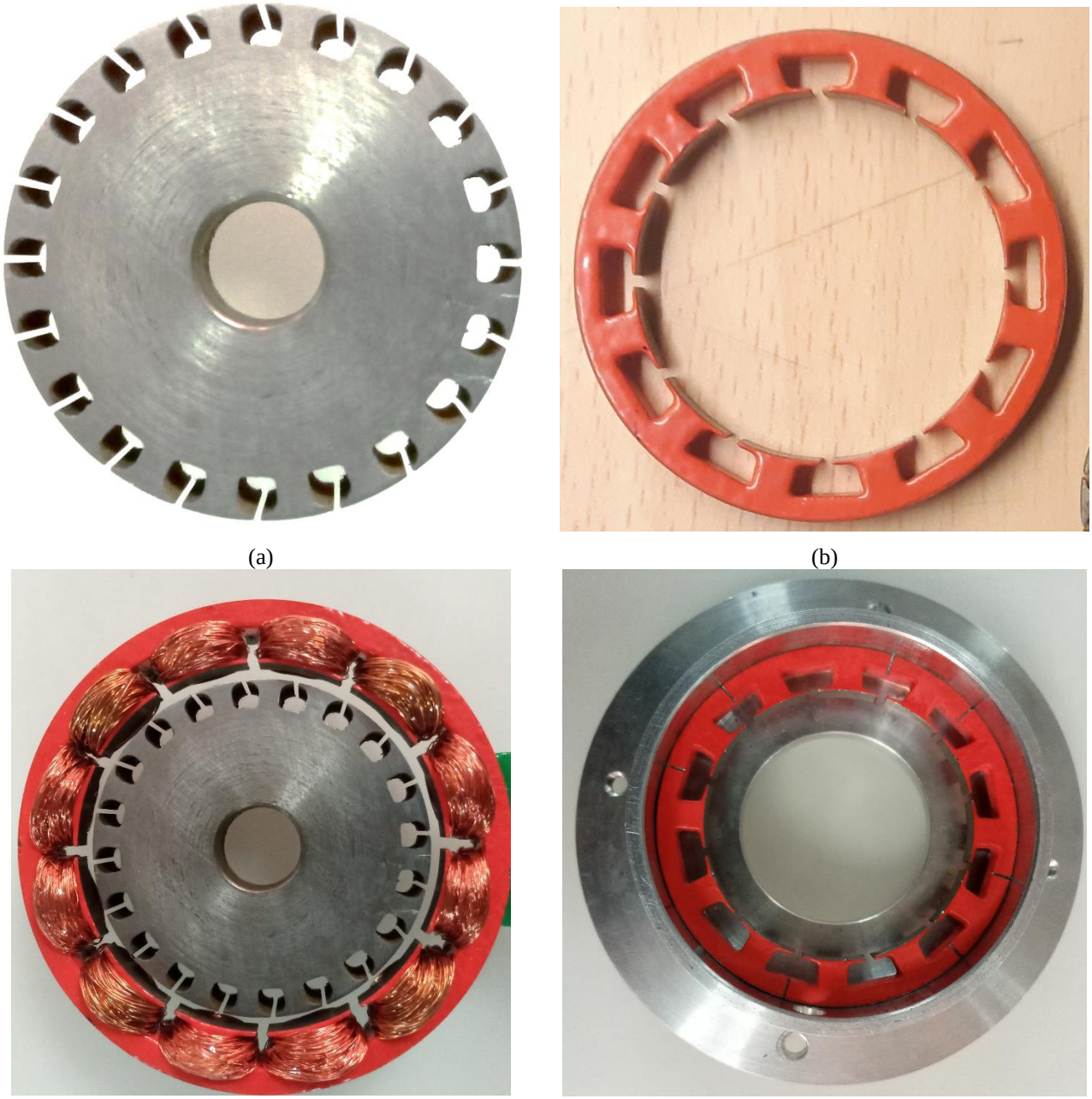

(a) (b)

(c) (d)

Fig. 11. The prototyped sensors:
(a) the rotor core before winding, (b) the rotor after winding, (c) the conventional stator, and (d) the discrete stator core

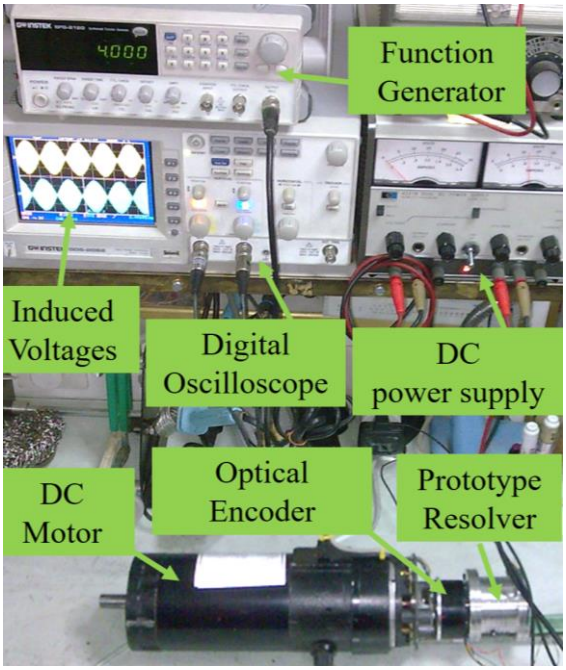

(a)

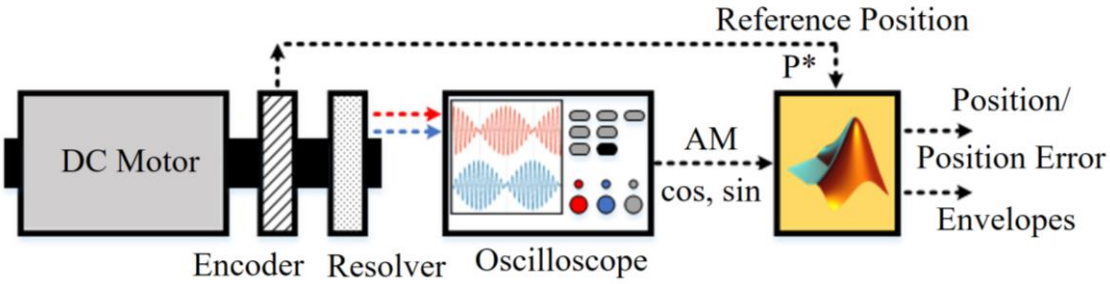

(b)

Fig. 12. Experimental test: (a) the employed test setup, and (b) the block diagram of the test circuit

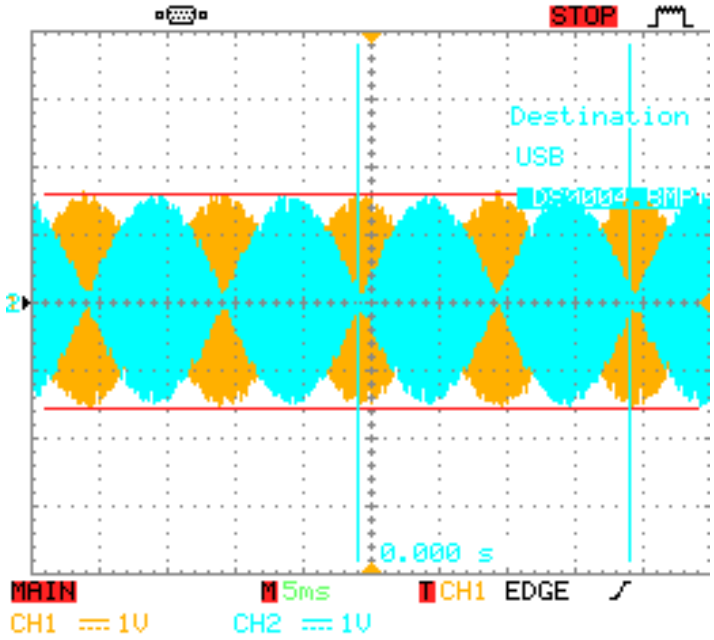
STOP
Destination
USB
DS0004.BMP
0.000 s
MAIN
M 5ms
T CH1 EDGE
CH1 1V
CH2 1V

(a)

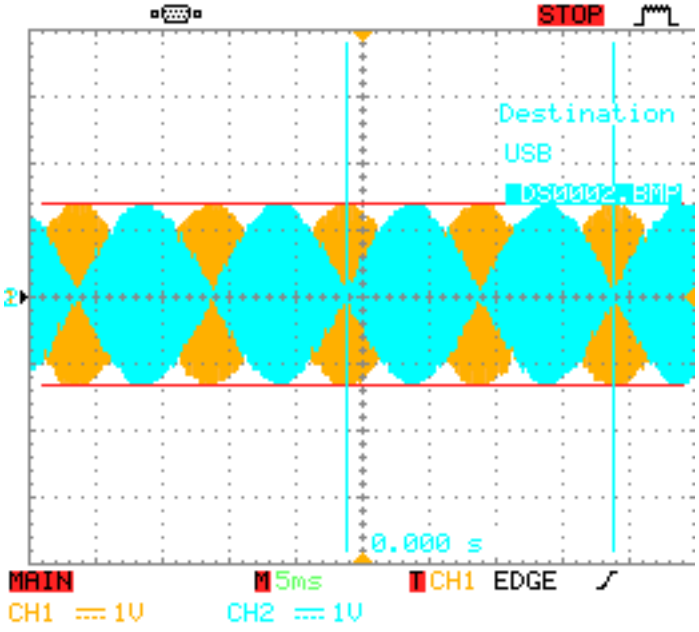
STOP
Destination
USB
DS0002.BMP
0.000 s
MAIN
M 5ms
T CH1 EDGE
CH1 1V
CH2 1V

(b)

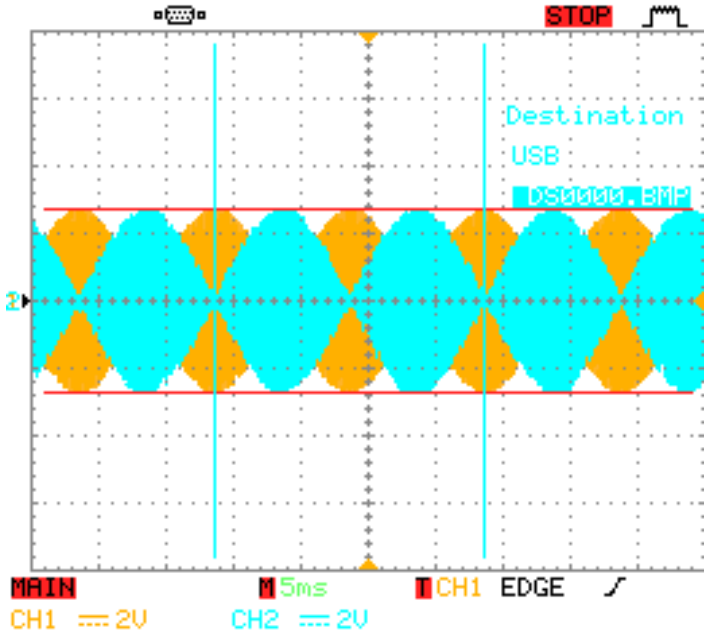

(c)

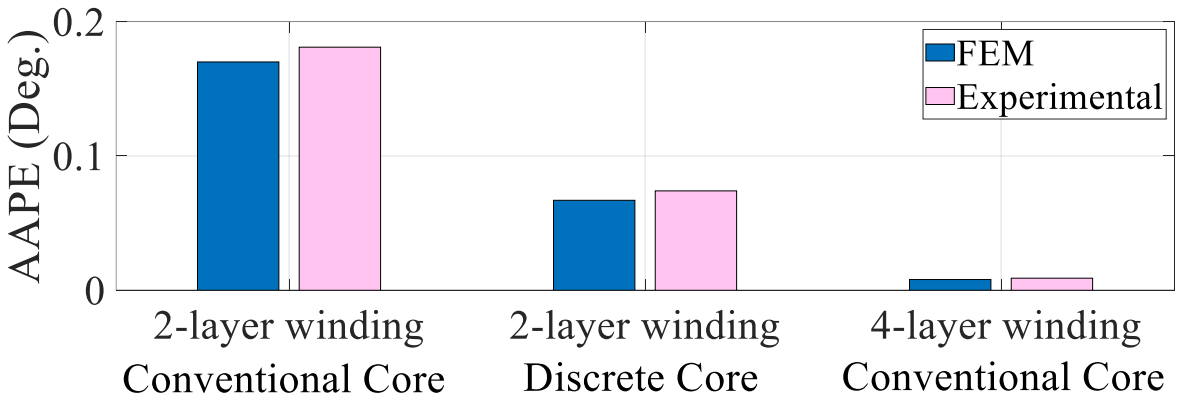

(d)

Fig. 13. The experimental results: (a) signal voltages of 2-layer winding with conventional core, (b) signal voltages of 2-layer winding with discrete core, (c) signal voltages of 4-layer winding with conventional core, and (d) comparing AAPE of prototypes with the simulation results

Table 1. Performance characteristic of different studied structures for 12-tooth, 10-pole WR resolver

Stator Winding	Stator Core	THD of envelopes (%)	The amplitude of the fundamental harmonic (V)	MPE (Deg.)	AAPE (Deg.)	PPPE (Deg.)	AAPE improvement with respect to conventional core	
							2-layer	4-layer
2-layer FSCW	conventional	2.296	1.5798	0.280	0.170	0.559	-	-
	1st structure	2.274	1.577	0.277	0.168	0.553	1.176%	-
	2nd structure	1.245	1.368	0.119	0.067	0.237	60.588%	-
	3rd structure	2.271	1.575	0.277	0.168	0.554	1.176%	-
4-layer FSCW	conventional	0.140	2.735	0.022	0.008	0.043	95.294%	-
	1st structure	0.134	2.727	0.023	0.007	0.045	95.882%	12.5%
	2nd structure	0.177	2.575	0.031	0.008	0.057	90.588%	0%
	3rd structure	0.138	2.727	0.022	0.007	0.044	95.882%	12.5%

Payam MohammadAli Rezayi was born in Urmia, West Azarbaijan, Iran. He received his B.S in electrical engineering (with first Hons.) from Urmia University, Urmia, Iran, in 2019 and his M.S in electrical engineering from Sharif University of Technology, Tehran, Iran, in 2022. His research interests include electrical machines, power electronics and its application in energy systems, modeling and control of power electronic converters and smart micro-grid systems.

Farid Tootoonchian received the B.Sc. and M.Sc. degrees in Electrical Engineering from the Iran University of Sciences and Technology, Tehran, Iran, in 2000 and 2007, respectively, and the Ph.D. degree from the K. N. Toosi University of Technology, Tehran, in 2012, all in electrical engineering. He is currently an Associate Professor at the Department of Electrical Engineering, Iran University of Sciences and Technology. His research interests include design, optimization, finite-element analysis, and prototyping of ultrahigh-speed electrical machines and ultrahigh-precision electromagnetic sensors.